Experiments testing the abatement of radiation damage in D-xylose isomerase crystals with cryogenic helium†

B. Leif Hanson,[a]* **Joel M. Harp,**[a] **Kristin Kirschbaum,**[b] **Constance A. Schall,**[c] **Ken DeWitt,**[c] **Andrew Howard,**[d] **A. Alan Pinkerton**[b] **and Gerard J. Bunick**[e]

[a]*University of Tennessee Oak Ridge Graduate School of Genome Science and Technology, PO Box 2009, Oak Ridge, TN 37831-8080, USA,* [b]*Department of Chemistry, University of Toledo, Toledo, OH 43606, USA,* [c]*Department of Chemical and Environmental Engineering, University of Toledo, Toledo, OH 43606, USA,* [d]*IMCA-CAT, APS, Argonne National Laboratory, Argonne, IL 60439, USA, and* [e]*Life Sciences Division, Oak Ridge National Laboratory, PO Box 2009, Oak Ridge, TN 37831-8080, USA. E-mail: blm@ornl.gov*

Helium is a more efficient cryogen than nitrogen, and for macromolecular data collection at high-flux beamlines will deliver lower temperatures. An open-flow helium cryostat developed at the University of Toledo (the Pinkerton Device) has been used for macromolecular data collection. This device differs from standard commercial He cryostats by having a much narrower aperture providing a high velocity stream of He around the crystal that maximizes convective and conductive heat exchange between the crystal and the cryogen. This paper details a series of experiments conducted at the IMCA-CAT 17ID beamline using one crystal for each experimental condition to examine whether helium at 16 K provided better radiation-damage abatement compared with nitrogen at 100 K. These studies used matched high-quality crystals (0.94 Å diffraction resolution) of D-xylose isomerase derived from the commercial material Gensweet SGI. Comparisons show that helium indeed abates the indicators of radiation damage, in this case resulting in longer crystal diffractive lifetimes. The overall trend suggests that crystals maintain order and that high-resolution data are less affected by increased radiation load when crystals are cooled with He rather than N_2. This is probably the result of a lower effective temperature at the crystal with concomitant reduction in free-radical diffusion. Other features, such as an apparent phase transition in macromolecular crystals at lower temperatures, require investigation to broaden the utility of He use.

Keywords: cryocrystallography; radiation damage; macromolecular crystallography.

1. Introduction

1.1. Cryocrystallography in synchrotron-based structural biology

Cryocrystallography has played an integral role in the success of synchrotron-based structural biology. In order to utilize the flux from these sources it is necessary to minimize the damage induced by X-radiation to crystalline samples. At cryogenic temperatures (below 150 K) at which the solvent becomes vitreous, radiation-induced free radicals are restricted in their migration through the crystalline biological material. This has allowed the development and proliferation of phasing techniques that use exhaustive sampling of the diffraction from a single crystal, such as multi- and single-wavelength anomolous dispersion (MAD and SAD), and the collection of ultrahigh-resolution (better than 1.1 Å) diffraction data sets.

Although the use of current cryocrystallographic techniques enormously reduces radiation damage to protein crystals, damage at 100 K is still significant in beams from third-generation synchrotrons. Radiation damage, of which deleterious manifestations in diffraction data include decreased resolution and increased mosaicity and crystal disorder (Ravelli & McSweeney, 2000), can prevent the collection of sufficiently complete data to solve the structure of a new protein using MAD or SAD phasing, or unambiguous determination of all atomic positions in an ultrahigh-resolution structure. The problem of radiation damage can adversely affect high-throughput structural studies and structure-based drug design. Consequently, the X-rays from third-generation sources generally have to be attenuated, limiting the utility and throughput of these incredibly powerful structural biology tools.

The immediate question of this study is whether cryogenics and cryocrystallographic techniques can be used to abate the damage that is induced by radiation exposure at a third-generation synchrotron beamline. Current crystal cooling techniques during data collection use the boil-off from liquid nitrogen to bathe the crystal in a cold gas stream. This usually results in a temperature of 90–100 K at the point of gas stream exit from the cryostat, 60–80 K higher than the temperature with open-flow He cryostats. Several factors presented in detail below contribute to the optimal cooling of a protein crystal during data collection. However, the easiest means of increasing the effective cooling at the crystal while using a cold gas stream is to change the cryogen from nitrogen to helium, although as a widely used strategy this would have financial and supply implications.

1.2. The case for cryogenic helium

Cooling of an object in a cold gas stream is the result of convective and conductive heat-transfer processes. When the crystal is exposed to the cold gas stream, the crystal surface temperature will decrease, causing internal conductive cooling in the outer crystal regions. As the cold front penetrates inward, more energy is conducted outward to the crystal surface to be convected away, and eventually the temperature at the center of the crystal is affected. The thermal and transport properties of helium are expected to lead to increased convective heat transfer.

The Pinkerton helium cryostat used in these studies differs from other currently available helium cryostats in several ways, one of which is the high velocity of the He stream from the small (1.5 mm diameter) nozzle opening of the device. These higher velocities can result in more efficient convective cooling of the crystal in comparison with conventional helium cryostats with wider nozzle openings and lower velocity streams. This results in a crystal that more closely approaches the cryogen temperature during data collection with an accompanying minimization of motion within the crystal lattice.

1.3. Macromolecular cryocrystallography using helium

Helium has been used sparingly in macromolecular studies because, until now, it was not clear whether the perceived benefit to macromolecular crystallography was real. The first specific experiments using He for cooling included the pioneering work of trapping the photo-reactive intermediates of carbon monoxide bound to heme (Schlichting *et al.*, 1994; Teng *et al.*, 1994). For these experiments, it was necessary to work at 40 K to slow the cycling of transient structure processes and prolong the lifetime of structural intermediates to a point where they were readily observable in diffraction data, thus necessitating He cooling. Several prototype He cryostats

were constructed during the course of these projects and have been used for other crystallography studies with cryogenic He (Teng & Moffat, 1998).

Our interest in helium cryogenics began with the development of a low-consumption open-flow helium cryostat at the University of Toledo (Hardie *et al.*, 1998). This device, originally developed for small-molecule charge density studies, was adaptable for macromolecular work since it allowed for the flash-cooling of crystals in the cold helium stream. Initial macromolecular studies have been made with a variety of X-ray sources, including sealed tube, rotating anode and synchrotron radiation. These results have enabled us to generate preliminary results for the value of cryogenic helium in reducing the effects of radiation damage, increasing the resolution and even its use for the flash-cooling of large crystals suitable for neutron diffraction studies (Hanson *et al.*, 1999, 2001).

Our preliminary studies on extended diffractive lifetime with He cooling were made at the 17ID beamline at the Advance Photon Source (APS) IMCA-CAT station at Argonne National Laboratory (Hanson *et al.*, 2001). Data were collected from a number of macromolecular crystal systems, including the nucleosome core particle, NCP (composed of approximately equal masses of protein and DNA), the human light chain dimer, Mcg, and the anti-ssDNA antibody Fab, BV0401, at an estimated temperature of 16 K based on previous calibrations using known phase transitions (Hardie *et al.*, 1998) and fluorescence lifetime measurements (Ribaud *et al.*, 2001). Observations of NCP revealed that after data collection in He the crystals were still clear, whereas after N_2 data collection (100 K) the crystals were blackened. In crystals of Mcg, the same $10°$ arc of the crystal was sampled for 90 min with helium cooling without a discernable decrease in the $I/\sigma(I)$ ratio for selected reflections. Data were collected from similar BV0401 crystals in both N_2 and He, and showed improved resolution and $I/\sigma(I)$ ratio for the He data. The N_2-cooled BV0401 crystal diffracted to 1.6 Å with an R_{merge} of 45.7% and $I/\sigma(I)$ of 1.4 in the highest-resolution shell. The He-cooled crystal diffracted to 1.48 Å with an R_{merge} of 34.2% and $I/\sigma(I)$ of 4.1 in the highest-resolution shell. Unfortunately, the radiation dose on the crystals for all these data-collection experiments at 17ID, although presumably similar, was unknown. A recent publication by Motoyama *et al.* (2002) saw similar resolution improvements moving from N_2 to He cooling at 40 K for data collected at BL14XU of SPring-8 with crystals of mutant scytalone dehydratase.

Although all these macromolecules have provided supporting evidence for advantages from helium use, we felt the most useful information for determination of radiation damage and increased lifetime would come from a series of dedicated radiation-damage experiments. With that goal in mind, studies were undertaken with D-xylose ketol-isomerase (XI, also known as glucose isomerase [E.C.5.3.1.5]) to determine if radiation damage could be abated with He as a cryogen, using simple diffraction statistics for comparison. Because the data-collection conditions for BV0401 in the previous series of experiments at IMCA-CAT 17ID were similar to those for the XI experiments reported here, the BV0401 data were reanalyzed to see if they conformed to the trends in the XI data. Once the XI data were analyzed and reduced, differences were examined between the refined molecular structure of the N_2-cooled crystal and that cooled with He to 16 K.

2. Methods and materials

2.1. XI purification and crystallization

XI was purified using protocols described by Dalziel (1999) from a commercial formulation of a genetically modified strain of *Strepto-* *myces rubiginosus* of the enzyme (Gensweet SGI) that was kindly provided by Genencor International (Rochester, NY, USA). This protein is especially attractive for these types of studies since it is available in large quantities (the sample provided by Genencor was over 10 g of protein), has well characterized solubility values (Dalziel, 1999) and has more medial values compared with other proteins with respect to size (43 kDa), pH of optimal activity ($\sim$7.8) and crystal solvent content ($\sim$50%). Most importantly, XI crystallizes readily in highly ordered crystals.

XI was purified from the commercial sample using a 4 ml aliquot ($\sim$0.3 g of protein) for starting material. The protein was separated from inhibitor (sorbitol) by precipitation in 7.5% (*w/v*) ammonium sulfate, followed by repeated washing of the precipitate with 20% (*w/v*) solution of ammonium sulfate. The purification of the sample can be followed by monitoring the color as the precipitate changes from brown to light tan. The precipitate was solubilized in 25 mM Tris, pH 8.0, and dialyzed against 25 mM Tris, 10 mM EDTA, pH 8.0, to remove any metal ions from the sample. After dialyzing out the EDTA, the sample was brought to crystallization trial conditions in 50 mM Tris, 2 mM MgCl$_2$, 2 mM CoCl$_2$, pH 8.0, and concentrated to 75 mg ml^{-1}. Hanging-drop crystallization experiments were made using 30 µl droplets of protein solution against 1 ml of 1.5 M ammonium sulfate, 50 mM Tris as reservoir solution.

2.2. Crystal selection, cryoprotection and data collection

Crystals of XI of similar size ($0.4 \times 0.4 \times 0.3$ mm) produced in the same well of hanging-drop crystallization experiments were harvested for data collection. Crystals were transported to IMCA-CAT at ambient temperature in an artificial mother liquor of 45% (*w/v*) ammonium sulfate, 0.1 M Tris, 2 mM MgCl$_2$, 2 mM CoCl$_2$. Cryoprotection with glycerol during flash-cooling was achieved by serial passing of the crystals for 30 s each through wells containing 5, 13, 20 and 30% (*v/v*) glycerol in 45% (*w/v*) ammonium sulfate, 0.1 M Tris solution. Direct transfer into 30% glycerol resulted in crystal cracking. All crystals were annealed using the macromolecular crystal annealing (MCA) protocol (Harp *et al.*, 1999) with the 3 min incubation occurring in the 30% (*v/v*) glycerol in 45% (*w/v*) ammonium sulfate, 0.1 M Tris solution after initial flash-cooling in the cold gas streams. No reciprocal cryogen-transfer experiments were attempted with these crystals; crystals flash-cooled in He stayed in He during data collection, as was the case for N_2-cooled crystals.

Data were collected at beamline 17ID at IMCA-CAT of APS with an ADSC Quantum 210 detector. For beamline 17ID, the flux incident on a 100×100 µm area at the protein sample position is close to 10^{12} X-photons s^{-1}. Ultrahigh-resolution data for XI were collected using $\lambda = 1.000$ Å radiation with both cold nitrogen (100 K) and helium (16 K) as cryogens, using one crystal for each cooling regime. For all data collection in both cooling regimes, the same exposure time (4 s per frame) and slit settings (200×200 µm) were used. For each crystal, two high-resolution (runs 1 and 2, detector distance 72 mm), one low-resolution (run 3, detector distance 144 mm), and one comparison data set (run 4, detector distance 72 mm) were collected. Runs 1, 2 and 3 sampled $100°$ using $0.5°$, 4 s ω scans, with runs 1 and 3 sampling the same space. The second high-resolution run (2) started $180°$ away from the beginning of the first high-resolution run (1). The comparison data (run 4) were collected after the collection of high- and low-resolution data (runs 1, 2, 3), and sampled the same portion of the crystal as the first high-resolution and the low-resolution runs (1 and 3) for $15°$, resulting in a fourth pass through the same region of the crystal. To minimize pixel overflow on

Table 1
Complete diffraction data statistics for N_2- and He-cooled D-xylose isomerase crystals (space group $I222$) used in later subset comparisons and for generation of difference maps.

Crystals used for both data sets were of similar size ($0.4 \times 0.4 \times 0.3$ mm). The values included in this table were derived by merging data-collection runs 1, 2 and 3 for each crystal.

	XI nitrogen cooled	XI helium cooled
Unit cell a (Å)	92.8	93.0
Unit cell b (Å)	98.0	98.1
Unit cell c (Å)	101.9	101.8
Volume (Å^3)	925977	928937
Reflections	323784	305039
Wilson B value (Å^2)	29.7	28.5
Overall completeness (%)	83.3	89.1
Highest-shell (1.04–1.10 Å) completeness (%)	53.1	70.2
Overall R_{merge} (%)	3.42	7.39
Highest-shell R_{merge} (%)	15.42	36.19
Overall $I/\sigma(I)$	47.3	34.7
Highest-shell $I/\sigma(I)$	2.3	3.2

Table 2
$15°$ subset comparison for ultrahigh-resolution xylose isomerase for N_2 and He data.

The number of contributing reflections is shown in parentheses after each run number. The highest-resolution shell for both the N_2 and He data was 1.04–1.10 Å.

	Volume	Wilson B (Å^2)	R_{merge} all shells (%) (high shell)	$I/\sigma(I)$ all shells (high shell)
Nitrogen data				
Run 1 (69530)	924557	30.9	3.16 (17.10)	30.1 (4.5)
Run 4 (71035)	926139	35.4	3.48 (37.00)	20.2 (1.8)
% 4 to 1	100.17	114.3	110.1 (216.4)	67.2 (39.7)
Helium data				
Run 1 (65449)	925530	31.6	3.96 (17.71)	28.6 (3.1)
Run 4 (65821)	932354	31.7	4.22 (22.54)	23.4 (2.9)
% 4 to 1	100.74	100.4	106.57 (127.3)	81.6 (95.4)

the CCD, aluminum-foil beam attenuation was 275 µm for runs 1, 2 and 4, and 675 µm for run 3.

The Pinkerton cryostat had a helium consumption of approximately 4 l of liquid helium per hour. The details of this cryostat design are discussed elsewhere (Hardie *et al.*, 1998). An Oxford Cryosystems Cryostream was used for the nitrogen-cooling experiments with a flow rate of 5 l of gas per minute measured at ambient conditions. The cryogen nozzle temperature was set to 100 K.

2.3. Data processing and refinement

The 1.000 Å wavelength ultrahigh-resolution diffraction data (both He and N_2) were processed with *Xgen* software (Howard, 1993). Statistical comparisons were made within and between the data sets. For consistency, the resolution cut-off for the 1.000 Å wavelength data was the detector side edge (1.04 Å). Both He and N_2 data sets provided data to 0.94 Å in the detector corners; however, these higher-resolution shells had less than 50% completeness. A future publication will detail the 0.94 Å structure of XI. Using the reduced data from the N_2 and He data sets to 1.04 Å resolution, $F_{o\mathrm{Nitrogen}} - F_{o\mathrm{Helium}}$ difference maps with a 6 Å resolution cut-off were generated using the *fo-fo_map* utility of the *CNS* software package (Brunger *et al.*, 1998). Model phases for this comparison were derived from the 1.6 Å resolution ambient temperature XI structure (PDB access number 1XIB) of Carrell *et al.* (1994). Molecular graphics were then generated with *Turbo-Frodo* software (Roussel & Cambillau, 1991).

3. Results

3.1. Statistical results for complete and subset diffraction data

Diffraction statistics for the two ultrahigh-resolution data sets are included in Table 1. The two data sets have similar unit cells and Wilson B values. Differences in completeness reflect the loss of individual frames as the result of shutter malfunctions during the N_2 data collection. Differences in R_{merge} and signal-to-noise ratio [$I/\sigma(I)$] are reflective of differences in the spot profile of the two data sets, described in more detail below.

Table 2 shows a comparison of the same $15°$ arc of data in the first and last runs of data collection from the same crystal using N_2 and He cooling. The table also includes the percentage change of each included value between runs 1 and 4. It was felt that the unit-cell volume was sufficiently sensitive to track changes in unit-cell parameters between the different data-collection runs. The highest-reso-

lution data shell diffraction statistics R_{merge} and $I/\sigma(I)$ are included, as well as the Wilson B value, which as a metric of crystalline disorder appears to have utility in tracking the effects of radiation damage. All of these values are available from the statistical output of the *Xgen* program. One value missing in these comparisons is the radiation load on the crystal. However, the radiation load for the helium and nitrogen runs being compared is the same within the confines of the fluctuations of the primary beam intensity since the beam width and frame times for all data collection were kept constant.

The improvements we have observed cannot be attributed to reduced absorption of the X-rays by helium compared with nitrogen. It should be noted that the path between the crystal and the detector is open to room air and not a closed environment. This open air is within a large APS X-ray hutch, where the air exchange is continuous and the relative enrichment of the atmosphere with cryogenic gas is negligible. Finally, the path length of the X-rays through either the cold He gas (1 mm half width of the He cold stream) or the N_2 (3 mm half width of the cold stream) is a much smaller distance than the distance traveled through room air. Based on a 72 mm crystal to detector distance, neither cryogen, even with the greater density of the cold N_2 (100 K) and He (16 K), contributes significantly to the X-ray absorbance for the distance traveled (*International Tables for Crystallography*, 1992, Vol. C, §4.2.4; Hartwig, 1998). Overall, the difference in absorption between the cold N_2 and the cold He is 0.39%. The absorption for the air path alone is ∼4.5%, and the overall difference in the transmittance between the two cryogenic conditions is 0.27%.

3.2. Manifestations of radiation damage and damage metrics

The most salient feature that emerges from Table 2 as a trend in the data is that the change for He data is significantly less than that for the N_2 data for the same number of frames. Manifestations of damage appear in Table 2 as a decrease of the signal-to-noise ratio in the highest-resolution shell and an increasing value of the Wilson B factor with increasing X-ray exposure. Thus, although the use of He does not prevent the effects of radiation damage appearing during crystal data collection, it does seem to provide a significant abatement of those effects, seen most markedly in the diffraction statistics for the highest-resolution data shells. These correlate well with our previous preliminary results suggesting that cryogenic helium can result in improved resolution and can also result in significant improvement in the crystal lifetime during data collection.

3.3. Spot splitting in He diffraction data

One difference between the N_2 and He data seen in Table 1 is the higher R_{merge} value for the He data. In the diffraction images of the XI He data, many of the reflections appear split. This spot splitting is shown in Fig. 1, where the three images are of reflections from the same frame at different resolutions. As can be seen in these images, the higher the resolution the more divergent the peaks within the spots appear. This is not the first time we have noted this phenomenon; it has appeared in all of our He-cooled diffraction data and was discussed by Hanson *et al.* (2001). We interpret these split spots as indicating a possible phase transition at these low temperatures (between 16 and 100 K) in the macromolecular crystals. Despite the problematic spot profiles, the He data were integrated as single observations. This allowed us to reduce the He data and use the resultant reflection data for comparisons between N_2 and He data sets.

4. Discussion

4.1. Comparison of crystal cooling with N_2 and He cryostats

During data collection the nozzle of the Pinkerton device was within 2–3 mm of the crystal; this is the closest approach possible without the cryostat nozzle casting a shadow on the detector. The abatement in radiation damage with cryogenic helium may be due to the lower crystal temperatures achieved with the 16 K helium stream compared with the 100 K nitrogen stream. From our preliminary analysis of heat-transfer coefficients, convective cooling is expected to be enhanced through the use of helium. This should result in maintenance of crystal temperatures closer to that of the cryogenic stream. As a first approximation, it will be assumed that conductive heat transfer is rapid in comparison with convective cooling. Properties of the crystal such as thermal conductivity and thermal diffusivity are needed to verify this assumption and are currently unavailable, but the assumption is expected to be valid under many operating conditions for very small crystal sizes of 100 μm or less average spherical diameter. The crystal is then assumed to exhibit no spatial variation in temperature and can be treated as a lumped system. Using an engineering approach to model this problem, a thermal energy equation written in lumped form for the crystal (Kuzay *et al.*, 2001) is

$$\rho_s V C_{ps} \frac{dT}{dt} = qV - hA(T - T_b), \tag{1}$$

where T is the crystal temperature, ρ_s is the crystal density, C_{ps} is the crystal heat capacity, V is the crystal volume, q is the volumetric rate of internal heat generation caused by incident X-rays, h is the convective heat-transfer coefficient, A is the crystal surface area and T_b is the temperature of the cryogenic stream of helium or nitrogen. This equation can be integrated analytically assuming constant crystal density, heat capacity and constant internal heat generation. The steady-state crystal temperature, T_s, is calculated from the integrated thermal energy equation and yields

$$T_s - T_b = qV/hA. \tag{2}$$

As the heat-transfer coefficient, h, increases in magnitude, the temperature difference between the crystal and cryogenic stream narrows with the crystal temperature approaching the cryogenic stream temperature. In practical terms, operating conditions that increase h will maintain crystal temperatures closer to the cryogen stream temperature.

Correlations for calculating h as a function of the dimensionless fluid Reynolds, Re, and Prandtl, Pr, numbers are widely used in engineering. In this system the gas stream corresponds to the fluid. These numbers are calculated from coolant properties and geometry:

$$\text{Re} = Dv\rho/\mu \qquad \text{and} \qquad \text{Pr} = C_p\mu/k, \tag{3}$$

where ρ is fluid density, μ is fluid viscosity, C_p is fluid heat capacity, k is fluid thermal conductivity and v is the average velocity of the flowing coolant stream. The quantity D is the equivalent diameter of the crystal. Use of heat-transfer correlations allows a comparison of convective heat transfer using different coolants and flow conditions. One such correlation for a spherical object immersed in a flowing stream (Brird *et al.*, 1960) is

$$hD/k = 2.0 + 0.6(Dv\rho/\mu)^{1/2}(C_p\mu/k)^{1/3}. \tag{4}$$

Using this correlation and the estimated velocity of the helium stream of the Pinkerton cryostat from its liquid-helium consumption, the heat-transfer coefficient of helium is calculated to be 3100 W m^{-1} K^{-1} for a crystal diameter of 0.20 mm. The heat-transfer coefficient of the nitrogen stream is estimated to be about 250 W m^{-1} K^{-1} for the same crystal dimensions. The velocity of the helium stream is estimated to be much greater than that of the nitrogen stream: 11.1 compared with 0.35 m s^{-1}. This difference alone would produce higher heat-transfer coefficients for the helium stream. However, calculating h using the lower nitrogen velocity yields a value of about 740 W m^{-1} K^{-1} for the helium stream. The
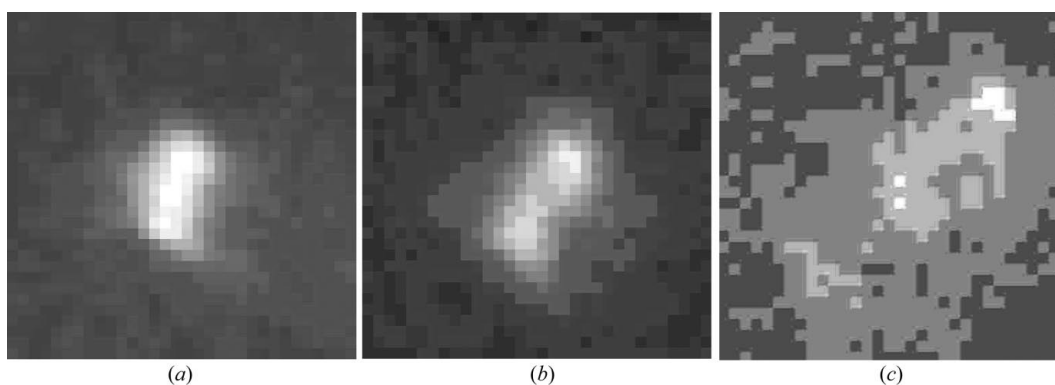

Figure 1
Split diffraction spot images from a 0.5° rotation frame of data collected from a 16 K He-cooled XI crystal. Pixel size is 51 × 51 μm. (*a*) 5.1 Å resolution reflection. (*b*) 2.3 Å resolution reflection. (*c*) 1.4 Å resolution reflection. All images were captured from a close-up window using the *HKL2000* software (Otwinowski & Minor, 1997).

higher value is due in large part to the higher thermal conductivity of helium (0.0228 W m^{-1} K^{-1}) than nitrogen (0.0096 W m^{-1} K^{-1}) at the operating conditions of the cryostats (Hartwig, 1998).

4.2. Trends in radiation-damage response between N$_2$- and He-cooled crystals

The composite trends for the two sets of data from XI crystals shown in Table 2 include greater increases in both the unit-cell volume and Wilson B metric with increased radiation load (increased time) for nitrogen-temperature data collection. For helium data, there is a lower R_{merge} and a much lower decrease in the signal-to-noise ratio in the highest-resolution shells with increased radiation exposure, compared with the data collected from the N$_2$-cooled crystal. Similar comparisons were extracted from diffraction data of crystals of BV0401, originally reported by Hanson *et al.* (2001). The results from the reprocessing of these data are shown in Table 3. The data from the two BV0401 crystals were similar in other diffraction measurements. The overall R_{merge} was 4.97% for the N$_2$ data and 5.21% for the He data; the overall $I/\sigma(I)$ ratios were also similar. The BV0401 results reinforce the XI observations: the overall trend suggests that crystals maintain order and high-resolution data are less affected by increased radiation load when crystals are cooled with He rather than N$_2$.

Although the diffraction statistics shown in Tables 2 and 3 appear to change as expected with increasing radiation damage, no single diffraction statistic or parameter appears to provide an unequivocal metric for radiation damage. Unit-cell parameters between data-collection runs can vary non-uniformly, as can mosaicity and highest-resolution shell statistics. A complex metric composed of the unit-cell parameters and diffraction statistics may provide a means of uniformly tracking radiation damage. Unfortunately, there are insufficient data in this study to determine the covariance with the parameter matrix. One facet of future studies will be the generation of more data for covariance analyses of diffraction parameters.

4.3. Phase transitions in macromolecular crystals cooled to helium temperatures

As mentioned above, the phenomenon of split spots has been observed in all of our cryogenic helium studies. Thus far we have been unable to determine whether the split-spot phenomenon is a new low-temperature phase transition, or the result of crystal splitting caused by the extreme temperature gradient that occurs when protein crystals are flash-cooled in a 16 K helium stream. The first explanation seemed the more likely, since crystals showed no cracks when visually inspected, nor did the crystal fragment when undergoing MCA. In our experience, crystals often fragment when warmed in cryoprotectant buffer if they become cracked during flash-cooling. In addition, the split-spot phenomena has been seen in all of our synchrotron experiments with the Pinkerton device, and has occurred in crystals sampled from a single well, from several wells that were part of one crystallization preparation, and from multiple crystallization experiments of one macromolecule. During the experiments described in this paper we were able to reposition the Pinkerton device cryostat head to where it will now be possible to recover crystals flash-cooled in He for data collection in N$_2$. Reciprocal experiments such as these should assist in establishing whether the split-spot phenomenon is the result of a low-temperature phase transition.

Other researchers have also observed the split-spot phenomena. Recently, the European Molecular Biology Laboratory – Institut Laue Langevin (EMBL-ILL) duplicated the phenomenon at the

Table 3
Comparison of high-resolution BV0401 data.

Runs 1 and 2 sample the same 10° arc of the crystal, similar to run 4 of the XI experiments. As with the XI experiments, the number of contributing reflections is shown in parentheses after the run number. The highest-resolution shell for the N$_2$ data was 1.60–1.68 Å; the highest-resolution shell for the He data was 1.49–1.53 Å. The two crystals used were collected from the same crystal mass and were of similar size ($0.3 \times 0.3 \times 0.1$ mm).

	Volume	Wilson B (Å^2)	R_{merge} all shells (%) (high shell)	$I/\sigma(I)$ all shells (high shell)
Nitrogen data				
Run 1 (20018)	217260	47.6	6.39 (47.45)	12.5 (1.3)
Run 2 (18554)	227685	55.7	6.42 (61.54)	11.4 (0.7)
% 2 to 1	104.80	116.9	114.84 (131.80)	90.6 (49.7)
Helium data				
Run 1 (10399)	222015	52.6	4.65 (30.85)	25.0 (1.8)
Run 2 (10669)	223210	51.9	4.82 (32.83)	21.4 (1.7)
% 2 to 1	100.54	98.8	103.66 (106.42)	85.5 (95.1)

DB21 neutron diffraction beamline in crystals initially flash-cooled in liquid nitrogen, then transferred to a Displex helium dilution refrigerator for cooling below 10 K (D. Myles, personal communication). Those observations corroborate ours, namely that a variety of protein crystals manifest these split diffraction spots at very low temperatures. At ILL, the most convincing diffraction data that displayed split spots were from crystals of myoglobin that were not initially twinned. The necessarily large crystals grown for neutron diffraction studies are often twinned; therefore special care is taken to identify twinning in the diffraction data. A Displex refrigerator cools by conduction; thus the time taken to reach minimum temperature is longer than in a cold gas stream. Lattice stresses within the cooled crystal should have a better opportunity to equalize when the crystal is cooled in this manner. Additionally, since these were neutron diffraction studies, they ruled out the possibility that the split-spot phenomenon is a consequence of low-temperature effects with X-rays, such as uneven crystal heating by the synchrotron beam causing variation in the lattice parameters within a single crystal. The low-temperature-induced split diffraction spot phenomenon observed by our group and at ILL also suggests that previously published results using helium for macromolecular data collection may not have achieved the $\sim$15 K temperatures obtained with a Displex or with the Pinkerton device.

To understand better what structural differences may occur between XI crystals cooled with N$_2$ and with He, 6 Å resolution difference density maps were generated from the diffraction data described in Table 1, based on the split diffraction spots of the He data integrated as a single component. The results of these maps are presented in Fig. 2. As is illustrated in Fig. 2(*a*), the majority of the differences (4σ) appear to be in the solvent shell around the protein. Fig. 2(*b*) demonstrates this in an even more marked fashion, showing the red 4σ difference density in a large solvent channel (40 Å across) within the crystal structure.

Several recent studies have examined the possibility of a low-temperature phase transition in amorphous water as one goes to very low temperature, with a light to heavy (more dense) transition described that can occur at 120 K or lower (Velikov *et al.*, 2001; Mishima & Stanley, 1998; Angell, 1995). This heavy phase is stable at standard pressure, although, in pure water, greater than standard pressure is required for its formation. At helium temperatures, the solvent with cryoprotectant in the flash-cooled crystals may have undergone a transition to the heavy vitreous water phase. A potential
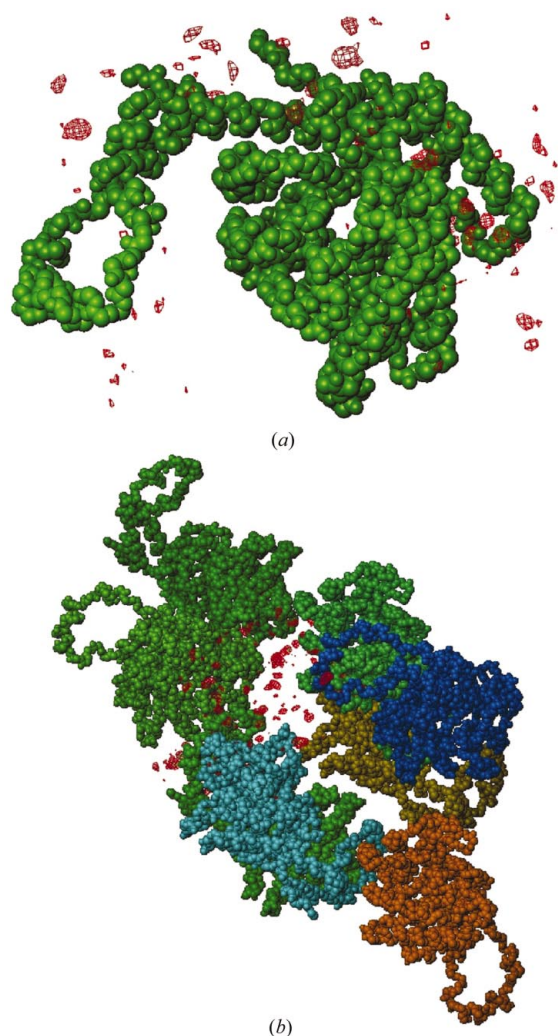
(a)

(b)

Figure 2
Structural differences between N_2- and He-cooled XI crystals. Using the PDB accession number coordinates from 1XIB (Carrell *et al.*, 1994) for model phases, maps of differences between the experimental data sets were generated using the *fo-fo_map* utility of *CNS* (Brunger *et al.*, 1998) from the two data sets statistically detailed in Table 1. (*a*) 4σ 6 Å resolution difference density in red for a single XI molecule. Note that most of the difference density appears outside the CPK model of the molecule. (*b*) 4σ 6 Å resolution difference density within a unit cell of an XI crystal. There is a large amount of difference density within the large (40 Å) solvent pore of the unit cell. Images were generated using *Turbo-Frodo* (Roussel & Cambillau, 1991).

mechanism for a heavy phase vitreous water transition in these crystals could be arrested expulsion of solvent in the low-temperature unit cell with the concomitant compaction of the lattice at low temperature resulting in some variability in unit-cell volume within the crystal. Slower cooling from the glass-transition to the helium temperature may alleviate this stress; however, the results with Displex refrigeration suggest that this is unlikely. Other factors that contribute to the difference map may be as prosaic as a difference in the uptake of glycerol cryoprotectant in the two different crystals. The possibility of ordered glycerol in the solvent structure may be low; however, it cannot be entirely dismissed.

4.4. Conclusions and future studies

The results presented here for XI indicate that the use of cryogenic He during data collection at a third-generation synchrotron source

results in an abatement of radiation damage compared with the results obtained from crystals cooled by cryogenic N_2. Helium is a better cryogen than N_2, leading to lower temperatures and faster heat transfer. Based on earlier work (Gonzalez & Nave, 1994; Burmeister, 2000; Weik *et al.*, 2000), which discussed the products and effects of radiation damage in detail, the improvements seen here are likely to be the result of decreased free-radical mobility at He temperatures.

When cooled to helium temperatures, the macromolecular crystals in this study appear to undergo a phase transition. The temperature at which this occurs is unknown, although it must be below 100 K. The similar results obtained from the Displex-cooling experiments on myoglobin suggest that the spot-splitting phenomenon/phase transition may be more general for macromolecular crystals at very low temperatures. Modulating the temperature to allow lattice relaxation should permit further characterization of the split-spot phenomenon, as will reciprocal flash-cooling–data-collection experiments (cooling in N_2, data collection in He and *vice versa*).

As identified in the previous sections, three areas will be the focus of immediate activities. The model for crystal cooling described in §4.1 will be refined in order to understand better what is happening to a protein crystal during flash-cooling and synchrotron X-ray exposure. Diffraction data will be collected from matched crystals to permit additional analyses of the diffraction parameters and crystal radiation load. Statistics from these analyses are needed to validate He-cooling benefits and to generate the appropriate radiation-damage metrics. Thermal control of the He cryostat will allow the determination of the spot-splitting transition temperature for a variety of protein crystals. Temperature cycling to allow lattice relaxation and knowledge of the low-temperature transition point will generate procedures to alleviate the occurrence of split diffraction spots.

Beyond these immediate objectives, long-range goals include exploration of the roles composition and concentration of solvents and cryoprotectants play on the durability of He-cooled crystals during X-ray data collection. The more mundane but no less essential engineering protocols for optimizing cooling and crystal handling in the cold He stream will also need to be addressed. Helium cooling will not be a panacea for radiation damage, but we believe it will become an established technique at macromolecular synchrotron beamlines.

References

Angell, C. A. (1995). *Proc. Natl Acad. Sci. USA*, **92**, 6675–6682.
Brird, R. B., Stewart, W. E. & Lightfoot, E. N. (1960). *Transport Phenomena*, p. 409. New York: John Wiley.
Brünger, A. T., Adams, P. D., Clore, G. M., DeLano, W. L., Gros, P., Grosse-Kunstleve, R. W., Jiang, J.-S., Kuszewski, J, Nilges, M., Pannu, N. S., Read,

R. J., Rice, L. M., Simonson, T. & Warren, G. L. (1998). *Acta Cryst.* D**54**, 905–921.

Burmeister, W. P. (2000). *Acta Cryst.* D**56**, 328–341.

Carrell, H. L., Hoier, H. & Glusker, J. P. (1994). *Acta Cryst.* D**50**, 113–123.

Dalziel, S. (1999). PhD thesis, University of Queensland, St Lucia.

Gonzalez, A. & Nave, C. (1994). *Acta Cryst.* D**50**, 874–877.

Hanson, B. L., Harp, J. M., Kirschbaum, K., Parrish, D. A., Timm, D. E., Howard, A., Pinkerton, A. A. & Bunick, G. J. (2001). *J. Cryst. Growth*, **232**, 536–544.

Hanson, B. L., Martin, A., Harp, J. A., Parrish, D. A., Kirschbaum, K., Bunick, C. G., Pinkerton, A. A. & Bunick, G. J. (1999). *J. Appl. Cryst.* **32**, 814–820.

Hardie, M. J., Kirschbaum, K., Martin, A. & Pinkerton, A. A. (1998) *J. Appl. Cryst.* **31**, 815–817.

Harp, J. M., Hanson, B. L., Timm, D. E. & Bunick, G. J. (1999). *Acta Cryst.* D**55**, 1329–1334.

Hartwig, G. (1998). In *Handbook of Cryogenic Engineering*, edited by J. G. Weisend. Philadelphia: Taylor and Francis.

Howard, A. J. (1993). *Am. Crystallogr. Assoc. Ann. Meet. Abstr.* C001.

Kuzay, T. M., Kazmierczak, M. & Hsieh, B. J. (2001). *Acta Cryst.* D**57**, 69–81.

Mishima, O. & Stanley, H. E. (1998). *Nature (London)*, **396**, 329–335.

Motoyama, T., Nakasako, M. & Yamaguchi, I. (2002). *Acta Cryst.* D**58**, 148–150.

Otwinowski, Z. & Minor, W. (1997). *Methods Enzymol.* **304**, 307–326.

Ravelli, R. B. & McSweeney, S. M. (2000). *Structure Fold. Des.* **8**, 315–328.

Ribaud, L., Wu, G., Zhang, Y. & Coppens, P. (2001). *J. Appl. Cryst.* **34**, 76–79.

Roussel, A. & Cambillau, C. (1991). *Silicon Graphics Partners Directory*, p. 86. Mountain View, CA: Silicon Graphics.

Schlichting, I., Berendzen, J., Phillips, G. A. Jr & Sweet, R. M. (1994). *Nature (London)*, **371**, 808–812.

Teng, T.-Y. & Moffat, K. (1998). *J. Appl. Cryst.* **31**, 252–257.

Teng, T.-Y., Srajer, V. & Moffat, K. (1994). *Nature Struct. Biol.* **1**, 701–705.

Velikov, V., Borick, S. & Angell, C. A. (2001). *Science*, **294**, 2335–2338.

Weik, M., Ravelli, R. B., Kryger, G., McSweeney, S., Raves, M. L., Harel, M., Gros, P., Silman, I., Kroon, J. & Sussman, J. L. (2000). *Proc Natl Acad. Sci. USA*, **97**, 623–628.